KSME

Springer

Journal of Mechanical Science and Technology 37 (2) 2023

Original Article
DOI 10.1007/s12206-023-0109-2

Keywords:
· High-speed elevator
· Coupling system
· Dynamic modeling
· Horizontal vibration
· Response analysis

Correspondence to:
Danlong Song
songdanlong@xaut.edu.cn

Citation:
Song, D., Zhang, P., Wang, Y., Du, C., Lu, X., Liu, K. (2023). Horizontal dynamic modeling and vibration characteristic analysis for nonlinear coupling systems of high-speed elevators and guide rails. Journal of Mechanical Science and Technology 37 (2) (2023) 643~653. http://doi.org/10.1007/s12206-023-0109-2

Received July 19th, 2022
Revised September 18th, 2022
Accepted October 25th, 2022

† Recommended by Editor
No-cheol Park

Horizontal dynamic modeling and vibration characteristic analysis for nonlinear coupling systems of high-speed elevators and guide rails

Danlong Song[1], Peng Zhang[1], Yuanhao Wang[1], Chunhua Du[1], Xiaomin Lu[2] and Kai Liu[1]

[1]School of Mechanical and Precision Instrument Engineering, Xi'an University of Technology, Xi'an 710048, China, [2]Hitachi Elevator (China) Co., Ltd., Guangzhou 511430, China

Abstract To study the horizontal vibration characteristics of high-speed elevators, a 6-DOF horizontal dynamic model of the nonlinear coupling system of guide rails, guide shoes, and elevator cabin was established. Four kinds of guide rail excitation models, namely, sinusoidal, triangular, stepped, and pulsed excitation, were established through an error and contact analysis of guide rails and rollers. The factors that influenced the horizontal vibration response, such as excitation models, stiffness of guide shoes, and cabin parameters, were analyzed by solving the vibration acceleration of the coupling system. Vibration acceleration was measured through experiments to verify the theoretical results. The vibration acceleration of the no-load elevator under stepped excitation was the largest. Reducing the stiffness of the guide shoes and straightness error of guide rails, reasonably arranging the spacing between the guide shoes at the top and bottom of the cabin, and increasing the cabin weight were beneficial to reducing the horizontal vibration response of the elevator cabin.

1. Introduction

With the acceleration of urbanization and the continuous emergence of high-rise and super-high-rise buildings, high-speed elevators as indispensable vertical transport tools are developing rapidly. Meanwhile, the requirements of consumers on riding safety, comfort, and energy efficiency are increasing. Vibration response is an essential index to evaluate the quality and comfort of elevators, so the maximum range of vibration acceleration is restricted by national standards [1]. Therefore, reducing the vibration of elevators has become an important technical difficulty. The running vibration of elevators mainly consists of vertical and horizontal vibrations [2, 3], and passengers are more sensitive to horizontal vibration than to vertical vibration [4]. With the increase in lifting height and velocity, horizontal vibration is becoming increasingly serious [5]; it considerably affects riding comfort and even threatens the safety of passengers. Thus, the horizontal dynamic modeling of the traction elevator cabin system was introduced to analyze the horizontal vibration characteristics and related influencing factors, thus providing a theoretical basis for reducing the horizontal vibration and improving the riding comfort of elevators.

In recent years, many studies have been conducted on similar types of problems. The horizontal vibration of high-speed elevators has been modeled and analyzed in depth. The horizontal vibration of elevators is mainly caused by defects in the guide rails and guide shoes and disturbances in the traction system and airflow [6-8]. In addition, external excitations, such as earthquakes and typhoons, affect the vibration and safety of elevators [9, 10]. Given the complexity of the elevator system, the cabin and frame are hypothesized as a whole rigid body when establishing a whole dynamic model [11, 12]. For example, in a previous study, a spatial dynamic model of the transverse vibration of an elevator cabin was established based on Newton's laws of motion and Euler equations [13]. An analytical method was presented to study an

initial boundary value problem describing transverse displacements under boundary excitation [14]. Depending on the focus, various dynamic models of horizontal vibration, such as 2-DOF [3, 15], 3-DOF [16], 4-DOF [8], 6-DOF [17], and 8-DOF [18], have been established. Previous studies have built a nonlinear model of rolling guide shoes on the basis of Hertz contact theory to consider the effect of guide shoes and rails [15, 20]. In addition, the influence of the migration of the centroid and elastic components between the cabin and frame was considered in dynamic modeling in Ref. [21]. However, most of these studies mainly analyzed the influence of the dynamic parameters of guide shoes on the elevator vibration response. The effects of the elasticity and damping of guide rollers have been ignored. The guide rail excitation model is too simple to reflect the actual vibration excitation.

Therefore, by investigating the dynamic parameters of guide shoes [22], this study aims to investigate the influence of elevator parameters and guide rail excitation on the horizontal vibration response. First, the contact stiffness of the guide rollers and rails was modeled based on Hertz contact theory. Second, a 6-DOF horizontal dynamic model of the traction elevator cabin system was established, and it included motion differential equations, a state space model, and excitation models of the guide rails. Lastly, horizontal vibration acceleration was solved with Matlab/Simulink. The influence of guide rail excitation and elevator parameters on the horizontal vibration response was analyzed and optimized comprehensively.

2. 6-DOF horizontal dynamic model of the cabin system

The traction elevator is a complex multi-body system. The vibration modes of running elevators, which are similar to those of the vehicle system, are numerous and highly complex; examples include floating, sinking, yawing, stretching, and rolling [12, 16]. The vibration in the horizontal direction can be divided into front-back vibration in the y-axis direction and transverse vibration in the x-axis direction, as shown in Fig. 1.

The horizontal vibration of the cabin system was mainly studied in this work. The vibrations in the *x*-axis and *y*-axis directions were similar. Therefore, the translation in the *x* direction and the rotation around the centroid on the *xoz* plane were comprehensively investigated. The four guide shoes were simplified into the same mass-spring-damper models. Then, a 6-DOF horizontal dynamic model of the cabin system was established, as shown in Fig. 2, where m_0 and J represent the total mass and moment of inertia of the cabin system, respectively; x and θ denote the horizontal displacement and rotation angle of the cabin system, respectively; m_1 is the mass of the guide shoe roller; k_1 and k_2 refer to the equivalent stiffness of the guide shoe roller and the spring stiffness of the guide shoe, respectively; c_1 and c_2 are the equivalent damping coefficients of the guide shoe roller and base, respectively; x_1, x_2, x_3, and x_4 are the horizontal displacements of the four guide shoes; u_1, u_2, u_3, and u_4 represent the irregular excitation displacements of guide rails at each guide shoe; and l_1 and l_2 are the distances between the centroid and guide shoes at the top and bottom of the cabin system in the *z* direction, respectively.

Table 1. Parameters of the specified elevator system.

J	l_1	l_2	m_a	m_b
6000 kg·m^2	2.0 m	1.5 m	2300 kg	10 kg
m_1	k_1	k_2	c_1	c_2
2 kg	400 N/mm	150 N/mm	0 N·s/m	1000 N·s/m

Note: m_a is the mass of the cabin and frame with half of the rated capacity (1000 kg). m_b is the mass of the guide shoe seat, so the total mass of the cabin system with four guide shoe seats is $m_0 = m_a+4m_b = 2340$ kg.

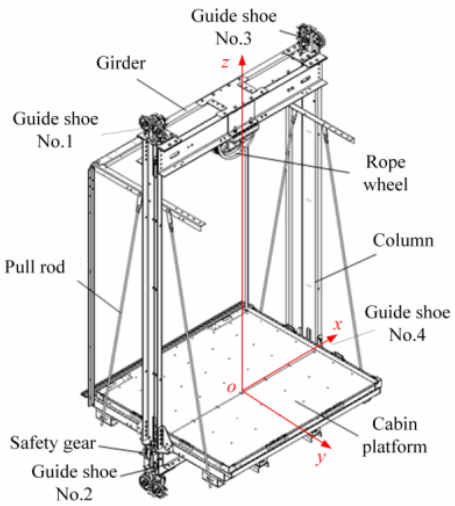

Fig. 1. Simplified model of the cabin system.

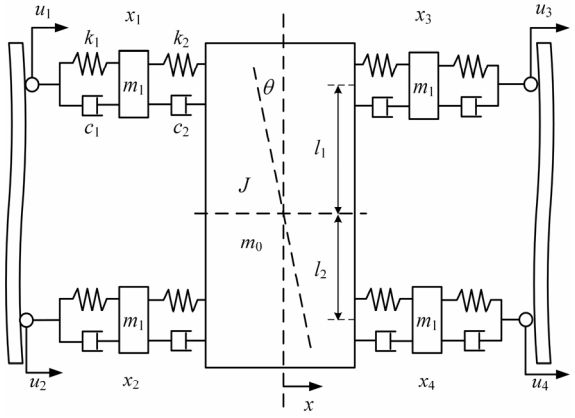

Fig. 2. 6-DOF horizontal dynamic model of the guide shoe-cabin system.

A specific elevator with half of the rated capacity was investigated as an example in this work. The rated capacity was 2000 kg, and the total mass of the cabin and frame was 1300 kg. The moment of inertia and centroid position were obtained with the 3D model of CAD. The detailed parameters of the specified elevator are shown in Table 1.

2.1 Differential equations of the cabin system

In accordance with D'Alembert's principle, a 6-DOF motion differential equation of the cabin system was established to comprehensively study the dynamic performance of the cabin system with guide shoes.

$$\begin{cases} m_0\ddot{x}_1 + k_1(x_1 - u_1) + c_1(\dot{x}_1 - \dot{u}_1) + k_2\left[x_1 - (x - l_1\theta)\right] + c_2\left[\dot{x}_1 - (\dot{x} - l_1\dot{\theta})\right] = 0 \\ m_0\ddot{x}_2 + k_1(x_2 - u_2) + c_1(\dot{x}_2 - \dot{u}_2) + k_2\left[x_2 - (x + l_2\theta)\right] + c_2\left[\dot{x}_2 - (\dot{x} + l_2\dot{\theta})\right] = 0 \\ m_0\ddot{x}_3 + k_1(x_3 - u_3) + c_1(\dot{x}_3 - \dot{u}_3) + k_2\left[x_3 - (x - l_1\theta)\right] + c_2\left[\dot{x}_3 - (\dot{x} - l_1\dot{\theta})\right] = 0 \\ m_0\ddot{x}_4 + k_1(x_4 - u_4) + c_1(\dot{x}_4 - \dot{u}_4) + k_2\left[x_4 - (x + l_2\theta)\right] + c_2\left[\dot{x}_4 - (\dot{x} + l_2\dot{\theta})\right] = 0 \\ m_0\ddot{x} + \left[k_2(x - l_1\theta - x_1) + c_2(\dot{x} - l_1\dot{\theta} - \dot{x}_1)\right] + \left[k_2(x - l_1\theta - x_3) + c_2(\dot{x} - l_1\dot{\theta} - \dot{x}_3)\right] + \\ \left[k_2(x + l_2\theta - x_2) + c_2(\dot{x} + l_2\dot{\theta} - \dot{x}_2)\right] + \left[k_2(x + l_2\theta - x_4) + c_2(\dot{x} + l_2\dot{\theta} - \dot{x}_4)\right] = 0 \\ J\ddot{\theta} + l_2\left[k_2(x + l_2\theta - x_2) + c_2(\dot{x} + l_2\dot{\theta} - \dot{x}_2) + k_2(x + l_2\theta - x_4) + c_2(\dot{x} + l_2\dot{\theta} - \dot{x}_4)\right] - \\ l_1\left[k_2(x - l_1\theta - x_1) + c_2(\dot{x} - l_1\dot{\theta} - \dot{x}_1) + k_2(x - l_1\theta - x_3) + c_2(\dot{x} - l_1\dot{\theta} - \dot{x}_3)\right] = 0 \end{cases} \tag{1}$$

The motion differential equation, Eq. (1), was transformed into a matrix form as follows:

$$\mathbf{M}\ddot{\mathbf{P}} + \mathbf{R}\dot{\mathbf{P}} + \mathbf{K}\mathbf{P} = \mathbf{Q}(t), \tag{2}$$

where **P**, **M**, **R**, **K**, and **Q**(t) represent the variable, mass, damping, stiffness, and guide rail excitation matrices, respectively.

$$\mathbf{P} = \begin{bmatrix} x & \theta & x_1 & x_2 & x_3 & x_4 \end{bmatrix}^{\mathrm{T}},$$

$$\mathbf{M} = diag\begin{bmatrix} m_0 & J & m_1 & m_1 & m_1 & m_1 \end{bmatrix},$$

$$\mathbf{R} = \begin{bmatrix} 4c_2 & 2c_2(l_2 - l_1) & -c_2 & -c_2 & -c_2 & -c_2 \\ 2c_2(l_2 - l_1) & 2c_2(l_1^2 + l_2^2) & c_2l_1 & -c_2l_2 & c_2l_1 & -c_2l_2 \\ -c_2 & c_2l_1 & c_1 + c_2 & 0 & 0 & 0 \\ -c_2 & -c_2l_2 & 0 & c_1 + c_2 & 0 & 0 \\ -c_2 & c_2l_1 & 0 & 0 & c_1 + c_2 & 0 \\ -c_2 & -c_2l_2 & 0 & 0 & 0 & c_1 + c_2 \end{bmatrix},$$

$$\mathbf{K} = \begin{bmatrix} 4k_2 & 2k_2(l_2 - l_1) & -k_2 & -k_2 & -k_2 & -k_2 \\ 2k_2(l_2 - l_1) & 2k_2(l_1^2 + l_2^2) & k_2l_1 & -k_2l_2 & c_2l_1 & -k_2l_2 \\ -k_2 & k_2l_1 & k_1 + k_2 & 0 & 0 & 0 \\ -k_2 & -k_2l_2 & 0 & k_1 + k_2 & 0 & 0 \\ -k_2 & k_2l_1 & 0 & 0 & k_1 + k_2 & 0 \\ -k_2 & -k_2l_2 & 0 & 0 & 0 & k_1 + k_2 \end{bmatrix},$$

$$\mathbf{Q}(t) = \begin{bmatrix} 0 \\ 0 \\ k_1u_1 + c_1\dot{u}_1 \\ k_1u_2 + c_1\dot{u}_2 \\ k_1u_3 + c_1\dot{u}_3 \\ k_1u_4 + c_1\dot{u}_4 \end{bmatrix}.$$

2.2 State space model

The state space approach is a theoretical calculation method with high stability and accuracy [23]. When the state space approach is used, the dynamic system is described by a first-order differential equation, which reveals the internal motion state and facilitates the processing of time-domain, nonlinear, multi-input, and multi-output systems. Therefore, the state space approach was used in this study to solve the horizontal vibration response of the cabin system. In accordance with the motion differential equation (Eq. (2)) that was linearized, the state space model of the cabin system was established as follows:

$$\begin{cases} \dot{\mathbf{X}} = \mathbf{A}\mathbf{X} + \mathbf{B}\mathbf{U} \\ \mathbf{Y} = \mathbf{C}\mathbf{X} + \mathbf{D}\mathbf{U} \end{cases}, \tag{3}$$

where **X**, **U**, **Y**, **A**, **B**, **C**, and **D** are the state variable, input variable, output variable, system, input, output, and direct transformation matrices, respectively.

$$\mathbf{X} = \begin{bmatrix} \dot{x} & \dot{\theta} & \dot{x}_1 & \dot{x}_2 & \dot{x}_3 & \dot{x}_4 & x & \theta & x_1 & x_2 & x_3 & x_4 \end{bmatrix}^{\mathrm{T}},$$

$$\mathbf{U} = \begin{bmatrix} u_1 & \dot{u}_1 & u_2 & \dot{u}_2 & u_3 & \dot{u}_3 & u_4 & \dot{u}_4 \end{bmatrix}^{\mathrm{T}},$$

$$\mathbf{A} = \begin{bmatrix} -\frac{4c_2}{m_0} & -\frac{2c_2(l_2-l_1)}{m_0} & \frac{c_2}{m_0} & \frac{c_2}{m_0} & \frac{c_2}{m_0} & \frac{c_2}{m_0} & -\frac{4k_2}{m_0} & -\frac{2k_2(l_2-l_1)}{m_0} & \frac{k_2}{m_0} & \frac{k_2}{m_0} & \frac{k_2}{m_0} & \frac{k_2}{m_0} \\ \frac{2c_2(l_2-l_1)}{J} & -\frac{2c_2(l_1^2+l_2^2)}{J} & -\frac{c_2l_1}{J} & \frac{c_2l_2}{J} & -\frac{c_2l_1}{J} & \frac{c_2l_2}{J} & \frac{2k_2(l_2-l_1)}{J} & -\frac{2k_2(l_1^2+l_2^2)}{J} & -\frac{k_2l_1}{J} & \frac{k_2l_2}{J} & -\frac{k_2l_1}{J} & \frac{k_2l_2}{J} \\ \frac{c_2}{m_1} & -\frac{c_2l_1}{m_1} & -\frac{c_1+c_2}{m_1} & 0 & 0 & 0 & \frac{k_2}{m_1} & -\frac{k_2l_1}{m_1} & -\frac{k_1+k_2}{m_1} & 0 & 0 & 0 \\ \frac{c_2}{m_1} & \frac{c_2l_2}{m_1} & 0 & -\frac{c_1+c_2}{m_1} & 0 & 0 & \frac{k_2}{m_1} & \frac{k_2l_2}{m_1} & 0 & -\frac{k_1+k_2}{m_1} & 0 & 0 \\ \frac{c_2}{m_1} & -\frac{c_2l_1}{m_1} & 0 & 0 & -\frac{c_1+c_2}{m_1} & 0 & \frac{k_2}{m_1} & -\frac{k_2l_1}{m_1} & 0 & 0 & -\frac{k_1+k_2}{m_1} & 0 \\ \frac{c_2}{m_1} & \frac{c_2l_2}{m_1} & 0 & 0 & 0 & -\frac{c_1+c_2}{m_1} & \frac{k_2}{m_1} & \frac{k_2l_2}{m_1} & 0 & 0 & 0 & -\frac{k_1+k_2}{m_1} \\ 1 & 0 & 0 & 0 & 0 & 0 & 0 & 0 & 0 & 0 & 0 & 0 \\ 0 & 1 & 0 & 0 & 0 & 0 & 0 & 0 & 0 & 0 & 0 & 0 \\ 0 & 0 & 1 & 0 & 0 & 0 & 0 & 0 & 0 & 0 & 0 & 0 \\ 0 & 0 & 0 & 1 & 0 & 0 & 0 & 0 & 0 & 0 & 0 & 0 \\ 0 & 0 & 0 & 0 & 1 & 0 & 0 & 0 & 0 & 0 & 0 & 0 \\ 0 & 0 & 0 & 0 & 0 & 1 & 0 & 0 & 0 & 0 & 0 & 0 \end{bmatrix},$$

$$\mathbf{B} = \begin{bmatrix} 0 & 0 & 0 & 0 & 0 & 0 & 0 & 0 \\ 0 & 0 & 0 & 0 & 0 & 0 & 0 & 0 \\ \frac{k_1}{m_1} & \frac{c_1}{m_1} & 0 & 0 & 0 & 0 & 0 & 0 \\ 0 & 0 & \frac{k_1}{m_1} & \frac{c_1}{m_1} & 0 & 0 & 0 & 0 \\ 0 & 0 & 0 & 0 & \frac{k_1}{m_1} & \frac{c_1}{m_1} & 0 & 0 \\ 0 & 0 & 0 & 0 & 0 & 0 & \frac{k_1}{m_1} & \frac{c_1}{m_1} \\ 0 & 0 & 0 & 0 & 0 & 0 & 0 & 0 \\ 0 & 0 & 0 & 0 & 0 & 0 & 0 & 0 \\ 0 & 0 & 0 & 0 & 0 & 0 & 0 & 0 \\ 0 & 0 & 0 & 0 & 0 & 0 & 0 & 0 \\ 0 & 0 & 0 & 0 & 0 & 0 & 0 & 0 \\ 0 & 0 & 0 & 0 & 0 & 0 & 0 & 0 \end{bmatrix},$$

$$\mathbf{C} = \begin{bmatrix} 0 & 0 & 0 & 0 & 0 & 0 & 1 & 0 & 0 & 0 & 0 & 0 \\ 0 & 0 & 0 & 0 & 0 & 0 & 0 & 1 & 0 & 0 & 0 & 0 \end{bmatrix},$$

$$\mathbf{D} = \begin{bmatrix} 0 & 0 & 0 & 0 & 0 & 0 & 0 & 0 \\ 0 & 0 & 0 & 0 & 0 & 0 & 0 & 0 \end{bmatrix}.$$

In addition, the state space model (Eq. (3)) of the horizontal

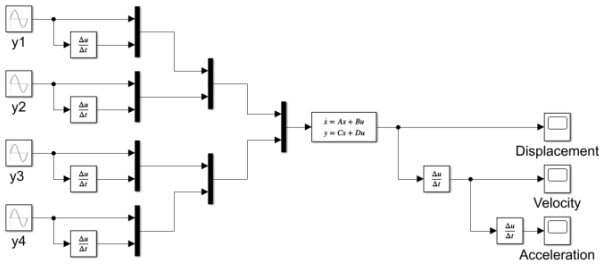

Fig. 3. State space model of the cabin system.

vibration differential equation of the cabin system was established in MATLAB/Simulink, as shown in Fig. 3.

2.3 Excitation models of guide rails

The surface profile and installation accuracy of guide rails are the most important factors that affect the horizontal vibration of elevators [8, 18]. Segmented guide rails are connected by the mortise and tenon and clamped by brackets. The tilt, step, and clearance of guide rail joints cause surface irregularity of guide rails. Guide rails produce periodic bending deformation that is similar to that of sinusoidal signals because of evenly spaced supports by brackets. Thus, the vibration excitation caused by the bending, skew, step, and clearance of guide rails can be simplified as sinusoidal, triangular, stepped, and pulsed excitation models, respectively, as shown in Fig. 4, where H and Δl represent the excitation amplitude and separation distance of adjacent brackets, respectively. According to the national standard of China [19], at least two brackets should be set for each guide rail with a spacing less than 2.5 m. In this work, the length l of a single guide rail with three brackets was 5 m, so Δl = 2.5 m.

The cabin system runs up and down along the guide rails on both sides under the support of the four guide shoes. We assumed that the displacement excitations of the four guide shoes were the same, but we set a specific period of time delay that was determined by the distance between the guide shoes at the top and bottom of the cabin.

$$t_0 = (l_1 + l_2)/v_0 , \tag{4}$$

where v_0 is the running velocity of the elevator.

For the sinusoidal excitation shown in Fig. 4(a), the excitation period is $T_a = 2\Delta l / v_0$. The displacement excitation at guide shoes No. 1 and No. 2 can be expressed as

$$\begin{cases} u_{1a} = H\sin[\omega(t+t_0)] \\ u_{2a} = H\sin(\omega t) \end{cases}, \quad t \in (0,+\infty) , \tag{5}$$

where the angular frequency is $\omega = \pi v_0 / \Delta l$.

For the triangular excitation shown in Fig. 4(b), the excitation period is $T_b = 4\Delta l / v_0$. The displacement excitation at guide shoes No. 1 and No. 2 can be expressed as

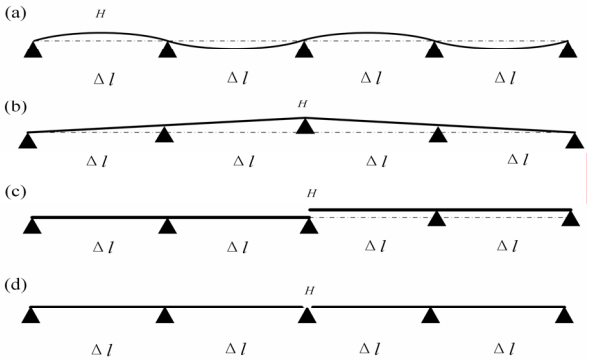

Fig. 4. Excitation models of guide rails: (a) sinusoidal excitation model; (b) triangular excitation model; (c) stepped excitation model; (d) pulsed excitation model.

$$\begin{cases} u_{2b}(t) = \dfrac{2H}{T}t - 2An, \quad (nT_b \le t \le nT + \dfrac{T_b}{2}, n \in N) \\ u_{2b}(t) = -\dfrac{2H}{T}t + 2H(n+1), \quad (nT_b + 2 < t < (n+1)T_b, n \in N) \\ u_{1b}(t) = u_2(t+t_0) \end{cases} . \tag{6}$$

For the stepped excitation shown in Fig. 4(c), the excitation period is $T_c = 4\Delta l / v_0$. The displacement excitation at guide shoes No. 1 and No. 2 can be expressed as

$$\begin{cases} u_{2c}(t) = 0, \quad (nT_c \le t \le nT + \dfrac{T_c}{2}, n \in N) \\ u_{2c}(t) = H, \quad (nT_c + \dfrac{T_c}{2} < t < (n+1)T_c, n \in N) \\ u_{1c}(t) = u_2(t+t_0) \end{cases} . \tag{7}$$

For the pulsed excitation shown in Fig. 4(d), the excitation period is $T_d = 2\Delta l / v_0$. The pulse width accounts for 2 % of the cycle period, so the displacement excitation at guide shoes No. 1 and No. 2 can be expressed as

$$\begin{cases} u_{2d}(t) = 0, \quad ((n+0.02)T_d < t < (n+1)T_d, n \in N) \\ u_{2d}(t) = H, \quad (nT_d \le t \le (n+0.02)T_d, n \in N) \\ u_{1d} = u_2(t+t_0) \end{cases} . \tag{8}$$

2.4 Bending deformation of guide rails

The guide rails were bent by the guide shoes with the elevator load. The contact area between the circular roller and the planar guide rail is shown in Fig. 5. r_0 = 80 mm, r_1 = 69 mm, and δ_r = 12 mm represent the outer radius, inner radius, and thickness of the guide roller, respectively. F_r is the normal contact force between the guide roller and rail, p is the Hertz contact pressure, and m is the half-width of the contact area. In accordance with Hertz contact theory, the stress distribution on the

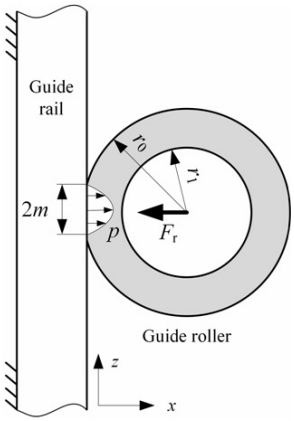

Fig. 5. Contact area of the guide roller and rail.

contact area was elliptical, and the maximum stress at the center was σ_{max}. Thus, the stress distribution of the contact area along the *z*-axis (guide rail direction) can be described as:

$$\sigma_{\mathrm{H}} = \sigma_{\max}\sqrt{1-\frac{z^2}{m^2}}\,. \tag{9}$$

The total contact force F_r integrated by stress distribution σ_H in the semi-elliptical cylinder is equal to

$$F_{\mathrm{r}} = \frac{\pi m}{2}\delta_{\mathrm{r}}\sigma_{\max}\,. \tag{10}$$

The contact radius of the linear guide rail is ∞, so the half-width *m* of the contact area can be derived from the Hertz equation as follows:

$$m = \sqrt{\frac{4F_r r_0}{\pi\delta_{\mathrm{r}}}\left(\frac{1-\nu_1^2}{E_1}+\frac{1-\nu_2^2}{E_2}\right)}\,, \tag{11}$$

where E_1, E_2, ν_1, and ν_2 are the elastic modulus and Poisson's ratios of the guide rollers and rails, respectively. The materials of the guide rollers and rails are resin rubber and Q235 steel, so E_1 = 20 MPa, E_2 = 206 GPa, ν_1 = 0.47, and ν_2 = 0.32.

By substituting Eq. (11) into Eq. (10), total contact force F_r can be expressed as:

$$F_{\mathrm{r}} = \sigma_{\max}^2\pi\delta_{\mathrm{r}}r_0\left(\frac{1-\nu_1^2}{E_1}+\frac{1-\nu_2^2}{E_2}\right). \tag{12}$$

The radial strain of the guide roller in the cylindrical coordinate system can be expressed as:

$$\varepsilon = \frac{\dfrac{r_0-\Delta x}{\cos\beta}-r_0}{r_0-r_1}\,,\quad \beta\in\left[-\arcsin\frac{m}{r_0},\arcsin\frac{m}{r_0}\right], \tag{13}$$

where Δ*x* represents the radial deformation of the guide roller

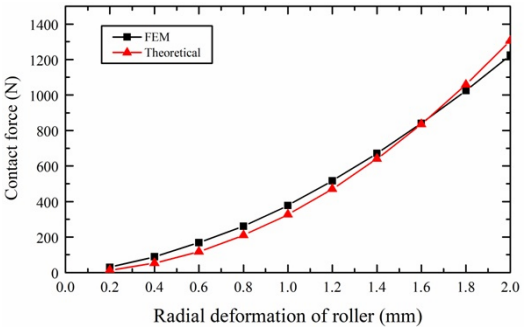

Fig. 6. Total contact force with various radial deformation of the guide roller.

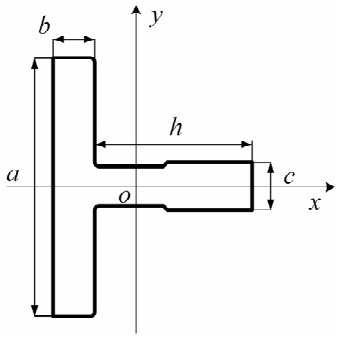

Fig. 7. Schematic of the T-type guide rail.

and β is the angle in the cylindrical coordinate system. The circumferential strain is equal to 0 due to the symmetry of the deformation. Thus, when β = 0°, the maximum stress σ_{max} at the center of the contact area can be described as:

$$\sigma_{\max} = E_1\varepsilon = E_1\frac{\Delta x}{r_0-r_1}\,. \tag{14}$$

By substituting Eq. (14) into Eq. (12), the curve of total contact force F_r varying with radial deformation was obtained and is shown in Fig. 6. The deformation of the guide roller was simulated via the linear elastic finite element method (FEM) of Abaqus. The contact force curves obtained by FEM and the theoretical equations were similar. To ensure the stability of elevators and the life of guide shoes based on positive engineering experience, the radial strain of the guide rollers was at most 0.1. The corresponding preload was about 500 N according to Fig. 6.

On the basis of the simple support condition of the guide rails and contact force F_r, the maximum bending deflection of the guide rails in the *x* and *y* directions can be expressed as:

$$\begin{cases} w_x = \dfrac{F_{\mathrm{r}}\Delta l^3}{48E_2I_x} \\ w_y = \dfrac{F_{\mathrm{r}}\Delta l^3}{48E_2I_y} \end{cases}. \tag{15}$$

The T-type guide rails shown in Fig. 7 are commonly used in

elevators. The moments of inertia, I_x and I_y, to the *x*-axis and *y*-axis of T-type guide rails can be calculated as

$$\begin{cases} I_x = \dfrac{1}{12}ba^3 + \dfrac{1}{12}hc^3 \\ I_y = \dfrac{ab^3}{12} + ab\cdot\left(\dfrac{ch(b+h)}{2(ab+ch)}\right)^2 + \dfrac{ch^3}{12} \\ \quad + ch\cdot\left[\dfrac{ch(b+h)}{2(ab+ch)} - \left(\dfrac{b+h}{2}\right)\right]^2 \end{cases} \tag{16}$$

where *a*, *b*, *c*, and *h* are the dimensions of T-type guide rails (Fig. 7).

In accordance with the dimensions of T-type guide rails, the moments of inertia relative to the *x*-axis and *y*-axis were set as $I_x = 1.08\times10^6$ mm^4 and $I_y = 7.51\times10^6$ mm^4, respectively. In accordance with the preload of 500 N, the bending deflections in the *x* and *y* directions were respectively set as $w_x = 0.73$ mm and $w_y = 1.05$ mm, which were the amplitudes of sinusoidal excitation.

3. Influencing analysis of the horizontal vibration of cabin system

According to the state space model, the horizontal vibration response of the cabin system is closely related to the input signal and state matrix. The input signal depends on the excitation model of guide rails. The state matrix is determined by the cabin system parameters. Thus, the effects of guide rail excitation and system parameters on horizontal vibration were analyzed in this section.

3.1 Effect of the excitation distribution mode

For guide rails on the left and right sides of the cabin system, the excitation distribution had three modes: parallel, symmetrical, and unilateral. We assumed that the excitation distribution of the guide shoes at the top and bottom on the same side was the same and only delayed by time t_0. The distribution mode and spacing of brackets on both sides of the guide rails were the same, so the amplitudes of the bending deflection of the guide rails were also the same.

1) When the displacement excitations of the guide rails on both sides were distributed in parallel, the bending directions of the guide rails on both sides were the same. The displacement excitations at guide shoes No. 3 and No. 4 can be expressed as

$$\begin{cases} u_3 = u_1 \\ u_4 = u_2 \end{cases}. \tag{17}$$

2) When the displacement excitations of the guide rails on both sides were distributed symmetrically, the bending of the guide rails on both sides was in opposite directions. The displacement excitation at guide shoes No. 3 and No. 4 can be expressed as

$$\begin{cases} u_3 = -u_1 \\ u_4 = -u_2 \end{cases}. \tag{18}$$

3) When the horizontal vibration of the cabin system was caused by the guide rail on one side, the other side guide rail was assumed to be an ideal line. Thus, the displacement excitation at guide shoes No. 3 and No. 4 can be expressed as

$$\begin{cases} u_3 = 0 \\ u_4 = 0 \end{cases}. \tag{19}$$

On the condition that the running velocity of the elevator was $v_0 = 2.5$ m/s, the amplitude of the sinusoidal excitation was $H = 1$ mm. The other detailed parameters are shown in Table 1. The horizontal vibration accelerations in the three modes were calculated with the Matlab/Simulink running state space model and are shown in Fig. 8.

According to the curves in Fig. 8, the acceleration response in the symmetrical distribution mode of guide rail excitation was zero. When the guide rails on both sides bent in opposite directions and the deflection was the same, the horizontal contact force of the guide rails on both sides was always the same, but the directions were opposite. Therefore, the horizontal resultant force acting on the cabin system was zero, so no horizontal vibration was generated. When the excitation distributions of the guide rails on both sides were parallel, the bending direction and deflection of the guide rails on both sides were the same. Thus, the horizontal contact force of the guide rails on both sides was always the same in direction and magnitude, and the acceleration response in the parallel excitation mode was twice that in the unilateral excitation mode. The errors of the guide rails on both sides can be superimposed to the guide rail on either side. In other words, the guide rail on one side can be assumed as an ideal line, and the other-side guide rail can be assumed as an irregular curve; the displacement excitation amplitude *H* is the sum of the deviations of the guide rails

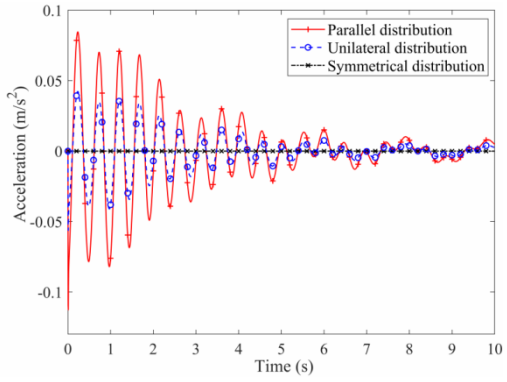

Fig. 8. Acceleration responses with various excitation distribution modes.

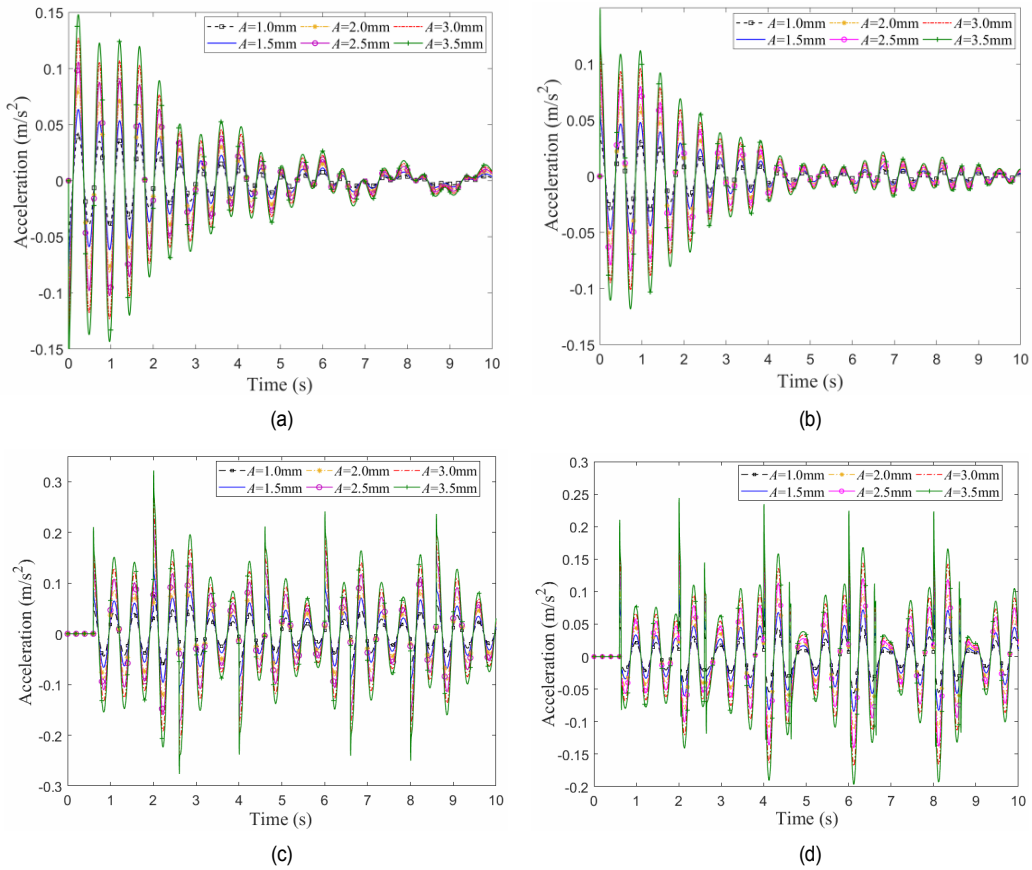

Fig. 9. Acceleration responses with various excitation models and amplitudes: (a) sinusoidal excitation; (b) triangular excitation; (c) stepped excitation; (d) pulsed excitation.

on both sides.

3.2 Effect of excitation model and amplitude

In accordance with the four types of excitation models and deflection of guide rails in Secs. 2.3 and 2.4 and the superposed deviations in Sec. 3.1, the excitation amplitude was set to H = 1.0-3.5 mm. The horizontal vibration acceleration with various amplitudes was solved and is shown in Fig. 9.

To compare the horizontal vibration acceleration of the different excitation models and amplitudes visually, the maximum peak-to-peak values of acceleration were integrated into Fig. 10. The single, double, stepped, and other excitations were studied. When the total amplitude of the excitations was constant, the maximum peak-to-peak values of acceleration increased linearly with the excitation amplitudes. When the amplitudes of sinusoidal, triangular, stepped, and pulsed excitations exceeded 2.03, 2.71, 1.28, and 1.92 mm, respectively, the maximum peak-to-peak values of acceleration were beyond the limit of 0.2 m/s^2 specified by the national standard of China [1]. In other words, stepped excitation affected the horizontal vibration of the cabin system the most when the excitation amplitude was constant. Therefore, stepped excitation can be used to analyze and design the vibration reduction of elevators. Meanwhile, the installation accuracy of guide rails must be guaranteed.

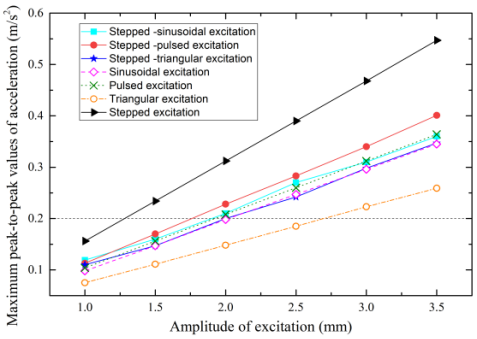

Fig. 10. Maximum peak-to-peak values of acceleration with various excitation models and amplitudes.

3.3 Effect of excitation frequency or running velocity

As mentioned above, stepped excitation had the greatest effect on the horizontal vibration of the cabin system in all kinds of excitation models. Therefore, stepped excitation was used to study the effect of excitation frequency on horizontal vibration

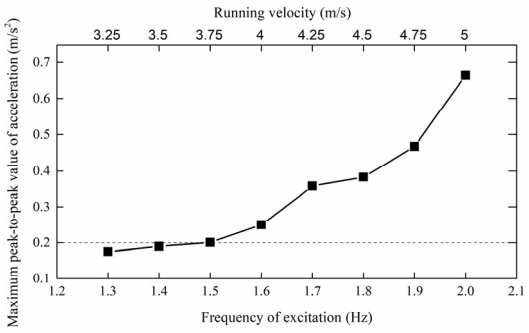

Fig. 11. Maximum peak-to-peak values of acceleration with various frequencies of stepped excitation.

in this section. The excitation frequency of guide rails depends on the running velocity of elevators. Thus, for the elevator developed by Hitachi Elevator (China) Co., Ltd., the frequency of stepped excitation varies from 1.3 Hz to 2.0 Hz when the range of the running velocity is 3.25-5 m/s. Then, the maximum peak-to-peak values of horizontal vibration acceleration with the stepped excitation amplitude of H = 1.0 mm were calculated and are shown in Fig. 11. The horizontal vibration acceleration increased with the frequency of stepped excitation and running velocity. Although the stepped error of the guide rail joints (amplitude H of stepped excitation) had a minimal value of 1.0 mm, the maximum peak-to-peak value reached the maximum allowable value of 0.20 m/s^2 when the excitation frequency was 1.5 Hz (the corresponding velocity was 3.75 m/s). Therefore, the installation accuracy of guide rails should be improved with the increase in running velocity.

3.4 Effect of cabin system parameters

According to system matrix **A** in Eq. (3), the total mass of the cabin system m_0 and the distances between guide shoes and centroid positions l_1 and l_2 are important system parameters that affect the vibration response. The spacing between the guide shoes at the top and bottom of the cabin $L = l_1+l_2$ affects the excitation phase of the guide shoes. Therefore, the effect of total mass m_0 and spacing L on horizontal vibration was analyzed under stepped excitation with an amplitude of H = 1.0 mm.

1) Effect of actual load on horizontal vibration

The actual load of the elevator varied from 0 kg to 2000 kg, where the range of the corresponding total mass m_0 was 1340-3340 kg. The horizontal vibration acceleration with various actual loads is shown in Fig. 12. The maximum peak-to-peak values of acceleration decreased with the actual load, which corresponded to the total mass of the cabin system. The maximum peak-to-peak value of acceleration was obtained when the elevator had no load. Therefore, the no-load state should be taken as the research condition when the horizontal vibration of elevators is studied.

2) Effect of spacing between guide shoes

The four guide shoes were symmetrically installed on both sides of the elevator cabin and rolled on the guide rails. Therefore, the spacing $L = l_1+l_2$ between the guide shoes at the top and bottom of the cabin determined the phases of the excitation model and the state variable matrix **X** in the state space model Eq. (3). The values of l_1 and l_2 varied synchronously when the effect of spacing $L = l_1+l_2$ on the horizontal vibration was analyzed. The cabin system centroid position fixed as spacing L changed. Thus, the centroid was assumed to be constant when investigating the relationship between spacing L and the excitation cycle caused by the guide rails. When spacing L varied from 3.20 m to 5.00 m according to the elevator developed by Hitachi Elevator (China) Co., Ltd., the corresponding excitation phase difference between the guide shoes at the top and bottom of the cabin was 1.3 π-2.0 π.

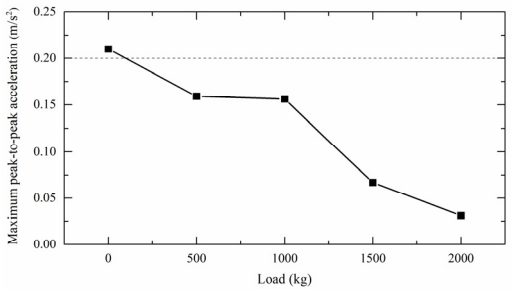

Fig. 12. Maximum peak-to-peak values of acceleration with various actual loads.

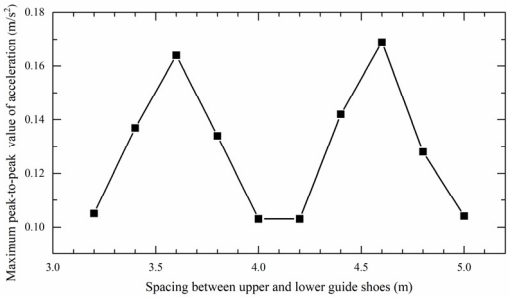

Fig. 13. Maximum peak-to-peak values of acceleration with various spacing between the guide shoes at the top and bottom of the cabin.

The maximum peak-to-peak values of acceleration response with various spacings are shown in Fig. 13. The acceleration response of horizontal vibration varied periodically with spacing between the guide shoes at the top and bottom of the cabin. When spacing L < 3.60 m, the acceleration response of horizontal vibration increased with the spacing. When spacing L > 3.60 m, the acceleration decreased with the spacing. When the spacing was 4.0-4.2 m, the acceleration response was at the minimum. Thus, on the condition of keeping the centroid position of the cabin system constant, the positions of the guide shoes at the top and bottom can be adjusted appropriately within a certain range to reduce the horizontal vibration of elevators.

3.5 Effect of guide shoe spring stiffness

To investigate the effect of the spring stiffness of guide shoes

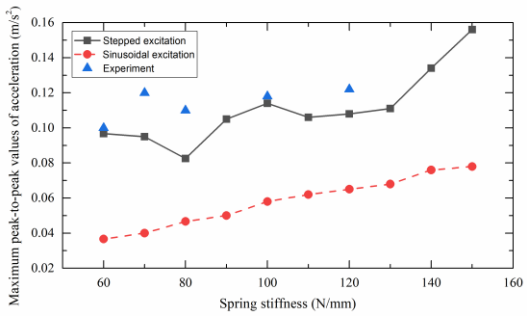

Fig. 14. Maximum peak-to-peak values of acceleration with various spring stiffness.

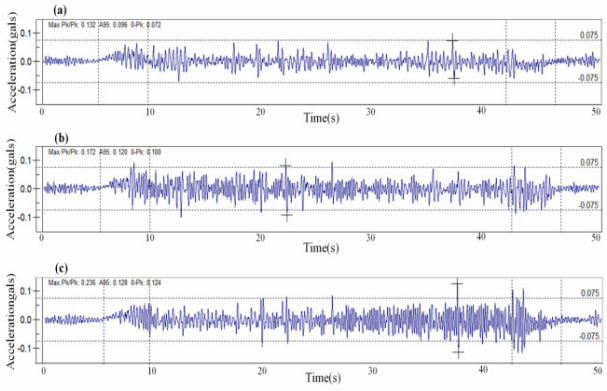

Fig. 15. Experimental measurement of horizontal vibration acceleration with various spring stiffness: (a) k_2 = 60 N/mm; (b) k_2 = 80 N/mm; (c) k_2 = 100 N/mm.

on horizontal vibration, the maximum peak-to-peak values of acceleration response with a range of spring stiffness k_2 = 60-150 N/mm were calculated and are shown in Fig. 14 on the basis of the elevator developed by Hitachi Elevator (China) Co., Ltd. The horizontal vibration acceleration was measured with the EVA-625 measurement system, which was developed especially for elevator vibration measurement by PMT Corporation of America, to verify the rationality of the horizontal vibration response analysis. The experiment was conducted in the test tower of Hitachi Elevator (China) Co., Ltd. The elevator started, ran, stopped, and ran again for 95 m from the 1st floor to the 30th floor at a velocity of 2.5 m/s and with half-load (1000 kg). The load was simulated by iron weights fixed on the floor and side wall of the elevator cabin. Three experiments were conducted on each spring stiffness of 60, 80, and 100 N/m by replacing the springs of the guide shoes. The acceleration sensor was fixed on the floor of the elevator cabin. Then, the average of three experimental values was regarded as the maximum acceleration and is shown in Fig. 14 with spring stiffness values of 60, 80, and 100 N/m.

Figs. 14 and 15 show that the spring stiffness of the guide shoes had a considerable influence on the horizontal vibration of the cabin system. The acceleration response increased with spring stiffness generally. However, the acceleration response with stepped excitation fluctuated locally, and the trend was consistent with the experimental measurement. The vibration response curves measured by EVA-625 in Fig. 15 are complicated because of the actual superimposed excitation of the guide rails. In addition, the bearing capacity of the guide shoes and the horizontal stability of the cabin system decreased with the reduction in spring stiffness. Therefore, the balance between vibration and stability needs to be considered.

4. Conclusions

A 6-DOF horizontal dynamic model and a state space model of the cabin system were developed to investigate the horizontal vibration characteristics. The factors that influence horizontal vibration were analyzed in terms of vibration excitation source (guide rails) and isolation target (cabin system) in detail. In essence, this work lays a theoretical foundation for suppressing horizontal vibration and improving riding comfort. The following conclusions were derived:

1) The effects of excitation models caused by guide rails, distribution modes, amplitudes, and frequencies were studied. The installation accuracy of guide rails affected horizontal vibration directly. Stepped excitation had the greatest influence on horizontal vibration, so the stepped errors of guide rail joints can be accumulated on one side and regarded as the primary excitation model to simplify the horizontal vibration analysis.

2) Horizontal vibration with various excitation frequencies (running velocities) and spring stiffness values of the guide shoes was investigated. The horizontal vibration acceleration increased with excitation frequency and running velocity. Therefore, the lower spring stiffness of guide shoes should be applied under the premise of ensuring the bearing stability of the cabin system.

3) The horizontal vibration varied periodically with the spacing between the guide shoes at the top and bottom of the cabin. The horizontal vibration was the largest when the elevator was empty.

Acknowledgments

This work was supported by the Natural Science Foundation of China (Program No. 51805429) and Young Talent Fund of University Association for Science and Technology in Shaanxi, China (20190416). The authors would like to acknowledge the editors and anonymous reviewers whose insightful comments have helped improve the quality of this paper considerably.

Nomenclature

m_0 and J : Mass and moment of inertia of the cabin system, respectively
m_a : Mass of the cabin and frame with half of the rated capacity (1000 kg)
m_b : Mass of guide shoe seats
x and θ : Horizontal displacement and rotation angle of the cabin system, respectively

m_1 : Mass of the guide shoe roller
k_1 : Equivalent stiffness of the guide shoe rollers
k_2 : Spring stiffness of the guide shoes
c_1 : Equivalent damping coefficients of the guide shoe rollers
c_2 : Equivalent damping coefficients of the guide shoe base
x_1, x_2, x_3, and x_4: Horizontal displacements of four guide shoes, respectively
u_1, u_2, u_3, and u_4: Irregular excitation displacements of guide rails at each guide shoe
l_1 and l_2 : Distances between the centroid and guide shoes at the top and bottom of the cabin system in the z direction, respectively
$\boldsymbol{P}$, $\boldsymbol{M}$, $\boldsymbol{R}$, $\boldsymbol{K}$, and $\boldsymbol{Q}(t)$: Variable, mass, damping, stiffness, and guide rail excitation matrices, respectively
$\boldsymbol{X}$, $\boldsymbol{U}$, $\boldsymbol{Y}$, $\boldsymbol{A}$, $\boldsymbol{B}$, $\boldsymbol{C}$, and $\boldsymbol{D}$: State variable, input variable, output variable, system, input, output, and direct transformation matrices, respectively
H and Δl : Excitation amplitude and separation distance of the adjacent bracket, respectively
v_0 : Running velocity of the elevator
ω : Angular frequency
r_0, r_1, and δ_r : Outer radius, inner radius, and thickness of guide rollers, respectively
F_r : Normal contact force between the guide roller and rail
p : Hertz contact pressure
m : Half-width of the contact area
σ_H : Stress distribution of the contact area
σ_{max} : Most significant stress at the center
E_1, E_2, v_1, and v_2: Elastic modulus and Poisson's ratios of guide rollers and rails
Δx : Radial deformation of rubber guide rollers
B : Angle of the cylindrical coordinate system
ω_x and ω_y : Maximum bending deformation of guide rails in the x and y directions, respectively
I_x and I_y : Inertia moments relative to x-axis and y-axis of T-type guide rails, respectively
A, b, c, and h : Dimensions of the T-type guide rails shown in Fig. 7
t_0 : Delayed time between the guide shoes at the top and bottom of the cabin on the same side
L : Spacing between the guide shoes at the top and bottom of the cabin

References

[1] National Technical Committee of Elevator Standardization, *Specification for Electric Lifts*, GB/T 10058-2009, Standards Press of China, Beijing, China (2009).

[2] Q. Peng, A. Jiang, H. Yuan, G. Huang, S. He and S. Li, Study on theoretical model and test method of vertical vibration of elevator traction system, *Mathematical Problems in Engineering*, 2020 (2020) 8518024.

[3] L. Qiu, Z. Wang, S. Zhang, L. Zhang and J. Chen, A vibration-related design parameter optimization method for high-speed elevator horizontal vibration reduction, *Shock and Vibration*, 2020 (2020) 1269170.

[4] H. Wu, D. Zhang and Q. Cheng, Modeling and parameter analysis on transverse vibration of the high-velocity elevator's hoisting system, *Journal of Machine Design*, 36 (6) (2019) 36-40.

[5] R. Zhang, C. Wang, Q. Zhang and J. Liu, Response analysis of non-linear compound random vibration of a high-speed elevator, *Journal of Mechanical Science and Technology*, 33 (1) (2019) 51-63.

[6] Y. Yamazaki, M. Tomisawa, K. Okada and Y. Sugiyama, Vibration control of super-high-speed elevators: car vibration control method based on computer simulation and experiment using a full-size car model, *JSME International Journal Series C*, 40 (1) (1997) 74-81.

[7] X. Li, C. Zhang, L. Li, G. Zhang and L. Guo, Influences of elevator guide rail on the cabin vibration, *China Mechanical Engineering*, 16 (2) (2005) 115-118+122.

[8] Z. Yang, Q. Zhang, R. Zhang and L. Zhang, Transverse vibration response of a super high-speed elevator under air disturbance, *International Journal of Structural Stability and Dynamics*, 19 (9) (2019) 1950103.

[9] D. Yang, K. Kim, M. K. Kwak and S. Lee, Dynamic modeling and experiments on the coupled vibrations of building and elevator ropes, *Journal of Sound and Vibration*, 390 (2017) 164-191.

[10] Y. Pan, Z. Li, C. Zhang and W. Shi, Elevator horizontal vibration response of a high-rise building under typhoon, *Journal of Vibration and Shock*, 34 (19) (2015) 103-108.

[11] J. Bao, P. Zhang, C. Zhu and W. Sun, Transverse vibration of flexible hoisting rope with time-varying length, *Journal of Mechanical Science and Technology*, 28 (2) (2014) 457-466.

[12] Q. Zhang, T. Hou, R. Zhang and J. Liu, Time-varying characteristics of the longitudinal vibration of a high-speed traction elevator lifting system, *The International Journal of Acoustics and Vibration*, 25 (2) (2020) 153-161.

[13] Y. Feng, J. Zhang and Y. Zhao, Modeling and robust control of horizontal vibrations for high-speed elevator, *Journal of Vibration and Control*, 15 (9) (2009) 1375-1396.

[14] N. V. Gaiko and W. T. van Horssen, Resonances and vibrations in an elevator cable system due to boundary sway, *Journal of Sound and Vibration*, 424 (2018) 272-292.

[15] S. Zhang, R. Zhang, Q. He and D. Cong, The analysis of the structural parameters on dynamic characteristics of the guide rail-guide shoe-car coupling system, *Archive of Applied Mechanics*, 88 (11) (2018) 2071-2080.

[16] D. R. Santo, J. M. Balthazar, A. M. Tusset, V. Piccirilo, R. M. L. R. F. Brasil and M. Silveira, On nonlinear horizontal dynamics and vibrations control for high-speed elevators, *Journal of Vibration and Control*, 24 (5) (2018) 825-838.

[17] M. Liu, R. Zhang, Q. Zhang, L. Liu and Z. Yang, Analysis of the gas-solid coupling horizontal vibration response and aerodynamic characteristics of a high-speed elevator, *Mechanics Based Design of Structures and Machines* (2021) DOI: 10.108

0/1539 7734.2021.1923525.
[18] J. Yin, Y. Rui, L. Jiang, B. Huang and Y. Li, Research on high-speed elevator MDOF horizontal dynamic characteristics and simulation, *Journal of Machine Design*, 28 (10) (2011) 70-73.
[19] National Technical Committee of Elevator Standardization, *Code for Acceptance of Electric Lifts Installation*, GB/T 10060-2011, Standards Press of China, Beijing, China (2011).
[20] R. Zhang, C. Wang and Q. Zhang, Response analysis of the composite random vibration of a high-speed elevator considering the nonlinearity of guide shoe, *Journal of the Brazilian Society of Mechanical Sciences and Engineering*, 40 (2018) 190.
[21] W. Fu, X. Liao and C. Zhu, Structural optimization to suppress elevator horizontal vibration Uusing virtual prototype, *Journal of System Simulation*, 17 (6) (2005) 1500-1504.
[22] D. Song, Y. Bai, X. Zhang, Y. Cui, K. Liu and X. Lu, Analysis and optimization of horizontal vibration isolation performance of elevator rolling guide shoes, *Journal of Machine Design*, 38 (1) (2021) 34-41.
[23] Y. Li, F. Xiong, L. Xie and L. Sun, State-space approach for transverse vibration of double-beam systems, *International Journal of Mechanical Sciences*, 189 (2021) 105974.

Danlong Song received his B.S. and Ph.D. degrees in aeronautics and astronautics manufacturing engineering from Northwestern Polytechnical University, China, in 2011 and 2016, respectively. He is currently an Associate Professor in the School of Mechanical and Precision Instrument Engineering, Xi'an University of Technology, China. His research interests include dynamics and structure optimization of mechanical systems and mechanical behavior of composite materials.